Structural, Mineralogical, and Rheological Properties of Methane Hydrates in Smectite Clays

Young-ju Seo,[†] Jiwoong Seol,[†] Sun-Hwa Yeon,[†] Dong-Yeun Koh,[†] Minjun Cha,[†] Sung-Pil Kang,[‡] Yu-Taek Seo,[‡] Jang-jun Bahk,[§] Jaehyoung Lee,[§] and Huen Lee*,[†]

Department of Chemical & Biomolecular Engineering, KAIST, 335 Gwahangno, Yuseong-gu, Daejon 305-701, Republic of Korea, Korea Institute of Energy Research, Daejeon 305-343, Republic of Korea, and Korea Institute of Geoscience & Mineral Resources, KIGAM, Gwahang-no 92, Yuseong-gu, Daejeon 305-350, Republic of Korea

Smectite clays are widely dispersed in deep ocean sediments and can be subdivided into two representative clay types, Cheto- and Wyoming-montmorillonites. In this study, we measured the thermodynamic phase behavior of methane hydrates intercalated at various concentrations of these clays and found the relatively weak promotion tendency when compared to that of pure methane hydrate stability. The structure and morphology of intercalated methane hydrate (IMH) samples were analyzed using the MAS NMR, RAMAN, LT-XRD, and Cryo-FE-SEM. The ^{27}Al and ^{29}Si solid-state MAS NMR spectra of IMH Cheto and Otay clays represent that the structural stability is preserved during the IMH formation, which is also indicated with the XRD pattern showing no structural transformation but different d-spacing values due to clay−water suspension and IMH. In addition, Cryo-SEM images of IMH samples show that IMH Otay clays provide well-developed methane hydrate (MH) morphology, compared to the IMH Cheto clay.

Introduction

Natural methane hydrates (MHs) have been found in ocean sediments under certain pressure and temperature conditions.[1] Most of the structure I (sI) methane hydrates in the deep-ocean environment are known to dominantly occur via a biogenic process. However, in a recent paper, Lu et al.[2] identified that the structure H (sH) hydrate exists in the natural environment, providing direct evidence of hydrate samples recovered from Barkley Canyon, on the northern Cascadia margin. They further demonstrated that sH is more stable than sI and may thus potentially be found in a wider pressure−temperature regime than are methane hydrate deposits. However, there is still a deficit of thermodynamic phase behavior and structural characteristics needed for understanding the physicochemical and mineralogical aspects of the natural formation of methane hydrates in marine sediments which generally coexisted with clay minerals. Among various clay minerals, the smectite group, otherwise known as montmorillonite, belongs to a 2:1 phyllosilicate composed of two tetrahedral sheets separated by one octahedral sheet.[3,4] In the smectite clays, there are two representative clay types, Wyoming- and Cheto-type montmorillonites, which differ primarily in the population of their octahedral layers, particularly regarding the amount of octahedral Mg.[3,5] In the Cheto-type montmorillonites, approximately one-fourth of the Al is replaced by Mg (average of 0.55 octahedral positions), and those Mg ions are regularly distributed in a hexagonal arrangement. On the other hand, the Wyoming-type montmorillonites have fewer Mg ions (average of 0.19 octahedral positions). Accordingly, the Cheto-type montmorillonite is thought to have a higher surface charge than the Wyoming-type montmorillonite due to its larger isomorphous substitutions in the octahedral sites, leading to ordered water adsorption in the clay−water system,[3,5] and water is readily incorporated into the interlayer space of clay sheets with an increase of clay volume, and this characteristic leads to the formation of dispersed methane hydrate deposits in a deep-sea enviroment.[4−6]

However, many molecular dynamic simulation studies of clathrate hydrates have focused on investigating the role of clay minerals in methane hydrate formation, while it has yet to be confirmed whether clay sediments play a specific role in shifting the hydrate formation conditions of intercalated methane hydrates (IMH) to a more favorable direction. Most of the modeling results lead to the conclusion that clay sediments promote hydrate formation.[7−9] On the contrary, reported experimental data can be divided into three patterns, promotion,[4,6] inhibition,[10−12] and no effect.[13,14] It might be attributed to diverse clay origins and physicochemical characteristics.

In this study, we sought to observe and identify the effect of hydrate formation on structural characteristics of clay minerals when methane hydrate was intercalated in the interlayer space of the Cheto-type montmorillonites, specifically, Cheto and Otay clays, because their suspensions show homogeneously a well-mixed state and good water adsorption. Hence, we anticipated well-mixed methane hydrate formation in Cheto-type clay minerals even at quite high clay concentrations. In particular, the mineralogical and rheological characteristics of marine sediment clays have a significant influence on the methane hydrate formation mechanism and moreover on the dissociation mechanism in sea floor sediments, which are currently becoming a vital topic to ensure the possibility of methane recovery from massive methane hydrate deposits in sea floor sediments. We also attempted to measure the methane hydrate equilibria in the montmorillonite interlayer, which greatly differ from those in dispersed clays. In addition, the effect of clay concentrations on shifting the phase equilibrium conditions was examined for

* Corresponding author. Tel.: 82-42-350-3917. Fax: 82-42-350-3910. E-mail address: h_lee@kaist.ac.kr.
[†] KAIST.
[‡] Korea Institute of Energy Research.
[§] KIGAM.

10.1021/je800833y CCC: $40.75
Published on Web 03/13/2009

Table 1. Mass Fraction of Wyoming- and Cheto-Type Montmorillonites

	Wyoming-type	Cheto-type	
compound	Wyoming (SWy-2) 100 W	Cheto (SAz-2) 100 W	Otay (SCa-3) 100 W
	Major Elements		
SiO_2	59.6000	60.9000	60.2000
Al_2O_3	22.8000	23.7000	22.1000
Fe_2O_3	4.7250	2.5400	2.6300
MgO	3.4000	5.8000	7.2000
CaO	1.1400	2.0300	0.6200
Na_2O	2.4508	0.1051	1.6608
K_2O	0.5490	0.2400	0.3500
TiO_2	0.1600	0.3350	0.3740
P_2O_5	0.0000	0.0000	0.0900
MnO	0.0360	0.1640	0.1130
Cr_2O_3	0.0170	0.0040	0.0120
S	0.1882	0.0440	0.0800
	Trace Elements		
Ni	0.0008	0.0008	0.0020
Cu	0.0144	0.0168	0.0210
Zn	0.0088	0.0096	0.0140
Sr	0.0340	0.0478	0.0180
Y	0.0032	0.0026	0.0040
Zr	0.0185	0.0407	0.0430
Nb	0.0031	0.0026	0.0030
Ba	0.0000	0.0027	0.0040
Sum	95.1488	95.9857	95.5388
LOSS[a]	4.8302		
Total	100.00		

[a] Loss notifies loss on ignition for early detection, and standard deviation (σ) is in a range of 0.01 to 0.05 for major components.

different clay types, which might provide valuable information for further molecular dynamic studies.

Experimental

Sample Preparations. Cheto-type montmorillonites (Cheto clay, *SAz-2*, AZ, USA, and Otay clay, *SCa-3*, *C*A, USA) and a Wyoming-type montmorillonite (Wyoming, *SWy-2*, Wyoming, USA) were obtained from the Source Clays Repository of The Clay Minerals Society. First, these samples were finely sieved and placed in a desiccator to prevent water uptake. CH_4 gas was supplied by Special Gas (Korea) and had a stated mole fraction purity of 99.9 %. Deionized water with ultrahigh purity was supplied from Merck (Germany). All materials were used without further treatments. The clay samples with various mass fraction contents (7.5 %, 25 %, 60 %, 80 % of clays as aqueous suspensions) were soaked in water and then ground until a viscous gel-like phase appeared in the well-mixed suspension. These samples were frozen at 203 K and then finely pulverized (< 150 μm) in a liquid nitrogen vessel. CH_4 gas supplied at the desired pressure and the temperature was controlled by an externally circulating refrigerator/heater (JEIO TECH, RBC-20).

Structural, Mineralogical, and Rheological Property Measurements. The structure and morphology of the intercalated MH samples were analyzed using the MAS NMR, RAMAN, LT-XRD, and Cryo-FE-SEM. A solid state NMR spectrometer (Bruker DMX 400 MHz NMR) was used to identify the chemical shift difference between intercalated and nonintercalated methane hydrate samples. The finely powdered samples were introduced into a 4 mm o.d. zirconia rotor loaded into a precooled NMR probe. All ^{13}C, ^{27}Al, and ^{29}Si NMR spectra were recorded at Larmor frequencies of (100.61, 104.23, and 79.46) MHz, respectively, with magic angle spinning (MAS) of about (5 to 7) kHz. A Raman spectrometer (Bruker RFS-100S Fourier transform-Raman spectrometer) was used with specially designed low-temperature attachments. The Raman spectra were determined using a InGaAs detector placed under a liquid nitrogen atmosphere. Exciting radiation was carried out with a Nd:YAG laser operated at 500 mw at a wavelength of 1064 nm. The 180 degree reflective sampling configuration was adjusted, and the resulting spectral resolution was 4 cm^{-1} with

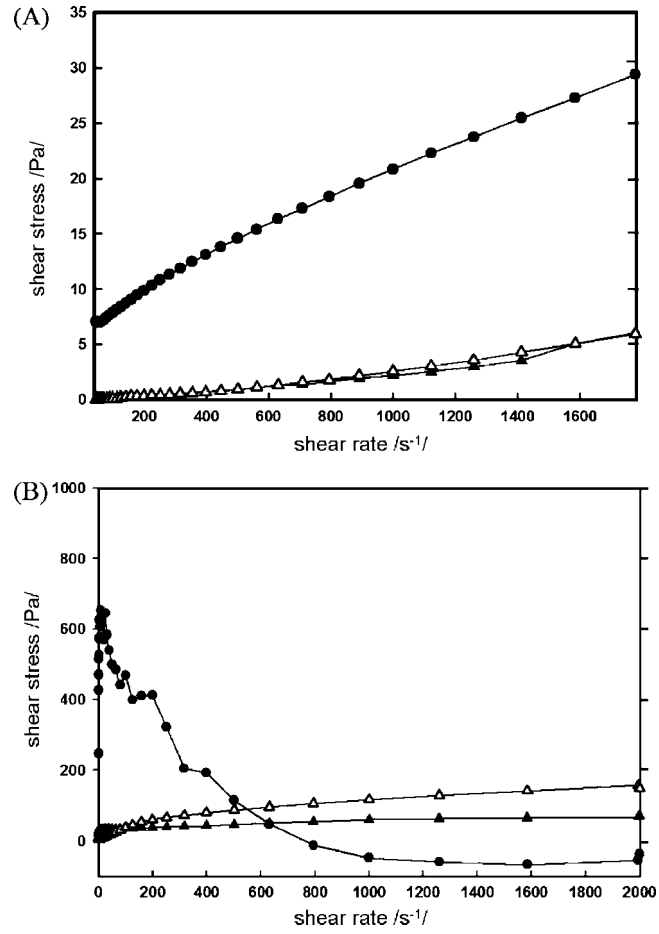

Figure 1. Rheograms of Wyoming-, Cheto-, and Otay-type montmorillonite suspensions at a clay mass fraction of (A) 10 % and (B) 40 % aqueous suspensions. ▲, Otay clay + H_2O; Δ, Cheto clay + H_2O; ●, Wyoming clay + H_2O.

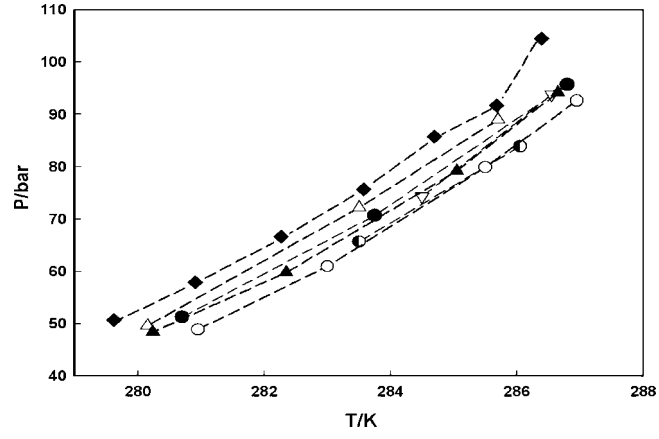

Figure 2. Hydrate phase equilibrium condition of Cheto and Otay clay CH_4 hydrates as a function of clay concentration. ◆, Pure CH_4 Hydrate; Δ, Cheto clay 7.5 wt % + CH_4 hydrate; ▲, Cheto clay 25 wt % + CH_4 hydrate; ▽, Cheto clay 60 wt % + CH_4 hydrate; ●, Otay clay 7.5 wt % + CH_4 hydrate; ○, Otay clay 25 wt % + CH4 hydrate; ◐, Otay clay 60 wt % + CH_4 hydrate.

Table 2. Physicochemical Properties of Cheto-Type Montmorillonites[a]

sample		Cheto-type montmorillonite	
		Cheto (SAz-2)	Otay (SCa-3)
surface area/$m^2 \cdot g^{-1}$	BET surface	36.4995	82.5328
	external surface	22.5554	48.4662
	internal surface	13.9440	34.0666
Particle size/μm	VMD	20.4540	16.4212
	SMD	7.5023	6.4704
	X_{50}	13.7102	10.5200
pore volume/$cm^3 \cdot g^{-1}$		0.0567	0.0794
pore average size/nm		6.2134	3.8486
* CEC/meq/100 g		120	125

[a] The sum of the BET surface includes both external and internal surfaces. VMD and SMD denote the volume mean distribution and the surface mean distribution. X50 denotes a half particle size of the cumulative distribution. CEC is the abbreviation of Cation Exchange Capacity. Data marked with an asterisk (*): information was obtained from Data Handbook for Clay Minerals produced by The Clay Minerals Society.

512 scanning steps. The LT-XRD patterns were recorded using a RIGAKU D/MAX-2500 X-ray diffractometer (Cu Kα, λ = 1.5406 Å). The system was operated at a step scan mode of 0.01°/1 s and 2θ in a range of (5 to 100) degrees at a working temperature of 203 K. The Cryo-Field Emission-Scanning Electron Microscopy images were obtained using a BALTEC MED 020 GBE (Freeze-Fracture/etching Cryo system) and HITACHI S-4700 (FE-SEM system) Scanning Electron Microscopy (SEM) with a beam energy of 10 kV at a low temperature of 203 K. The samples for the low-temperature SEM were prepared following the typical Cryo-ultramicrotomy technique that enables observation of the flat frozen surface. The specific surface area and pore volume and size were determined using a gas adsorption analyzer (model: Tristar 3000, Micromeritics, USA) and a particle size analyzer (model: Helos/Quixel, Sympatec, UK). For the measurements of mineralogical properties and composition analysis of clay samples, we used a parallel plate rheometer (model: Ares 4, Rheometric Scientific), XRF (model: MiniPal 2, Panalytical), and ICP-AES (model: Polyscan 60E, Thermo Jarrell). The approximately 25 cm^3 volume of the clay + water mixture was initially charged into the equilibrium cell to determine the P, T hydrate equilibria. The air in the cell was eliminated with flushing gas several times. The pressure was first adjusted to a desired pressure with gas. The cell temperature was kept constant at a temperature just above the methane hydrate formation temperature, and the system pressure then reached a steady state. The external heater was used to increase the system temperature at a rate of 0.2 K per hour. When the system temperature was kept constant for at least (8 to 10) h after the system pressure was stabilized, the pressure was considered a hydrate dissociation pressure at the specific temperature. For gas release measurements, the clay + methane hydrate formation proceeded for 5 days, and 1 g of the sample was charged into the 15 cm^3 cell previously cooled with liquid nitrogen. Next, the cell was put into the water bath (288 K), and the amount of gas release was measured by water substitution after (8 to 10) h.

Results and Discussion

Mineralogical Properties and Thermodynamic Phase Behavior of IMH. In a clay−water system, the clay particles carry a net negative charge on the surface due to isomorphous

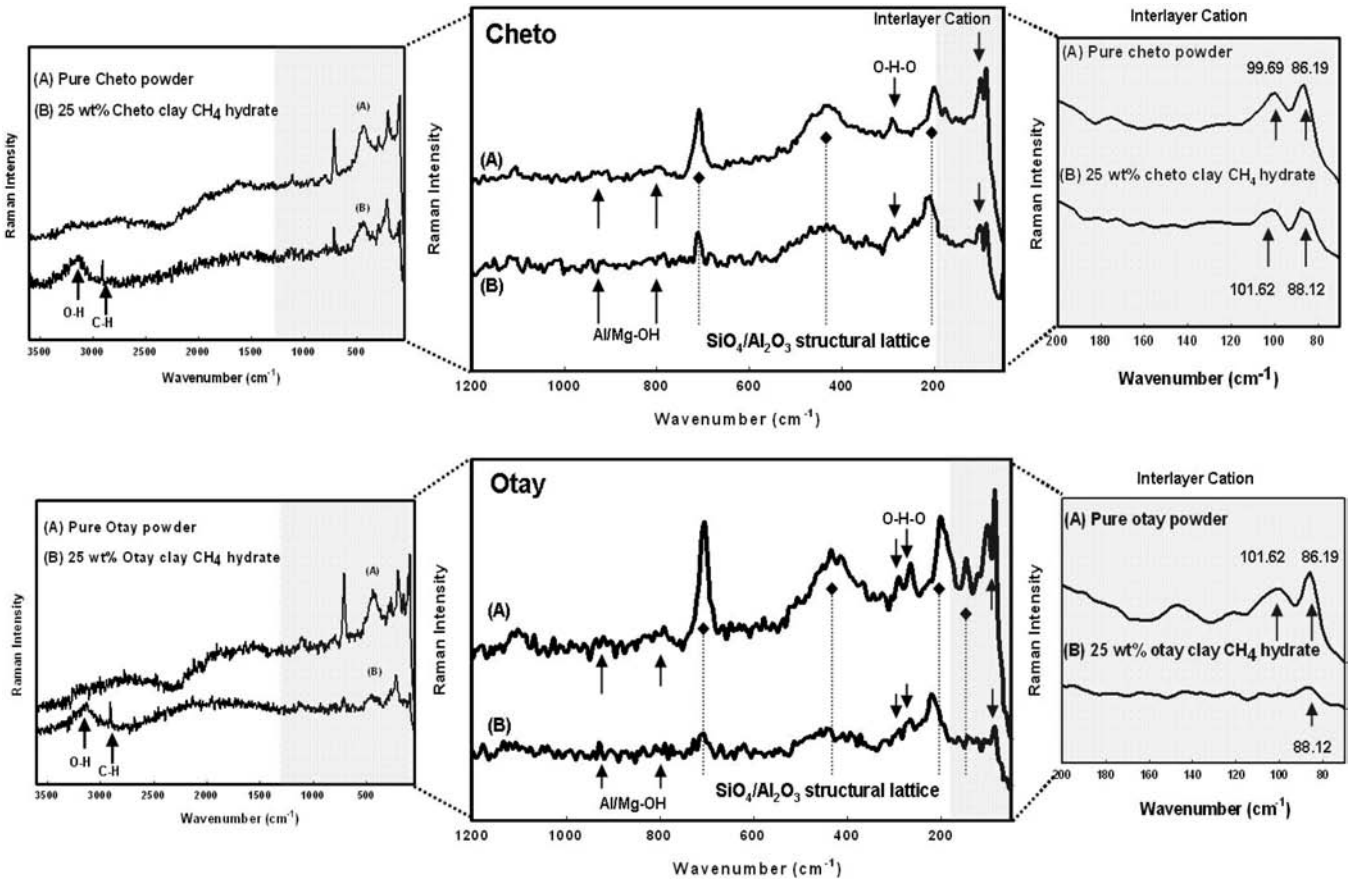

Figure 3. FT-Raman spectra of pure Cheto and Otay clay powders and mass fraction of 25 % clay CH_4 hydrates over a range of (3600 to 50) cm^{-1} at low temperature.

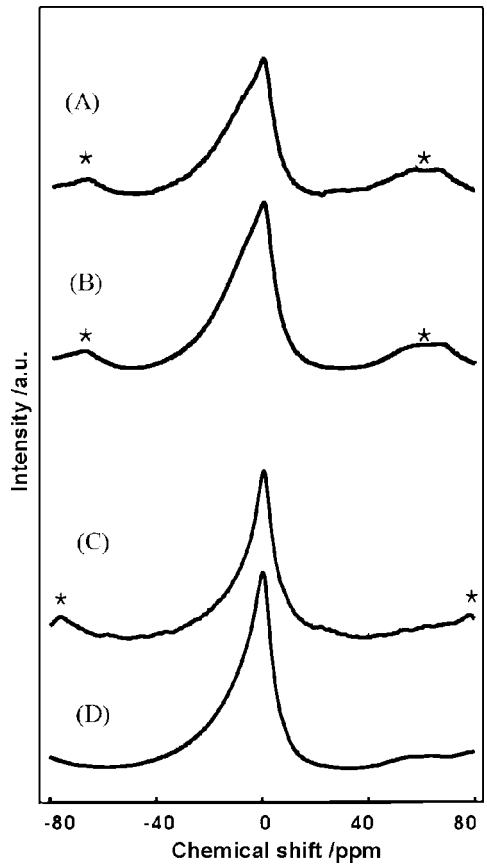

Figure 4. Solid state ^{27}Al MAS NMR spectra of pure Cheto and Otay clay powders and mass fraction of 25 % clay CH_4 hydrates. (A) Mass fraction of 25 % cheto CH_4 hydrate, (B) pure cheto-clay powder, (C) mass fraction of 25 % otay CH_4 hydrate, and (D) pure otay-clay powder. Asterisk-marked peaks are sideband.

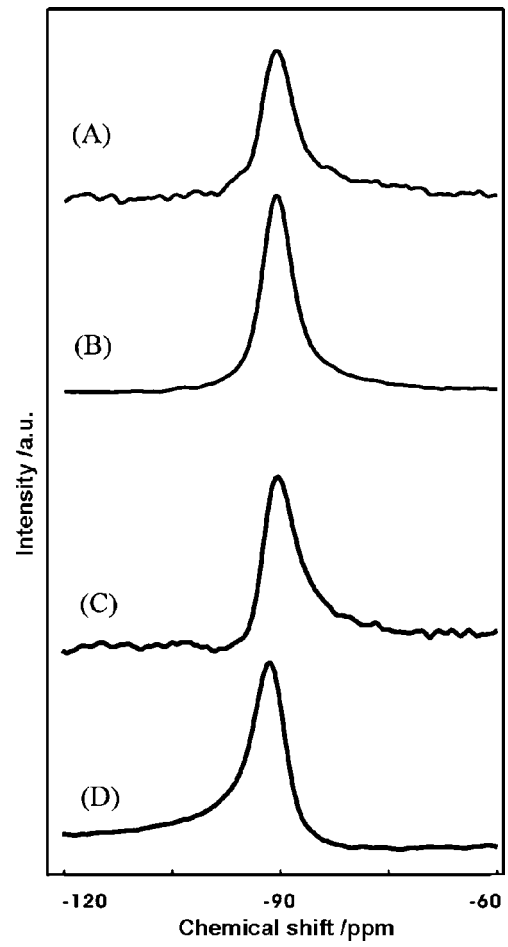

Figure 5. Solid state ^{29}Si MAS NMR spectra of pure Cheto and Otay clay powders and mass fraction of 25 % clay CH_4 hydrates. (A) Mass fraction of 25 % cheto CH_4 hydrate, (B) pure cheto-clay powder, (C) mass fraction of 25 % otay CH_4 hydrate, and (D) pure otay-clay powder.

substitution in the octahedral sheets in which the interlayer cations float around.[15] Mineralogically, the Cheto-type montmorillonite is known to have both a relatively high surface charge and a large surface area. As such, it provides strong ordered water adsorption providing a very favorable pathway for methane hydrate formation. To make a comparison of the chemical compositions, Wyoming- and Cheto-type montmorillonites were analyzed and are listed in Table 1. Volzone and Garrido reported that the Na^+ content of montmorillonites is the principal factor in determining the clay's rheological properties.[16,17] As shown in Figure 1, the viscosities of the two clay suspensions differ substantially, even at the same clay concentration. The Wyoming-type clay suspension is highly viscous with a thixotropic property, while the rheological behavior of the Cheto-type montmorillonite follows a Newtonian fluid. From the experiments, we observed that the Wyoming-type clay is not well mixed at a clay mass fraction above 45 %. On the contrary, the Cheto-type montmorillonites are well suspended, facilitating methane hydrate formation in the clay interlayer space even at high clay concentration.

The hydrate stability and phase equilibrium in clay minerals differ greatly from those in the bulk hydrate owing to surface and capillary effects in the clay pores. It has been confirmed that hydrate formation in the confined pores is severely restricted due to increased inner capillary pressure. Furthermore, in principle, the clay particles suspended in water play a negative role in structuring the crystalline hydrate. These two physical reasons provide a basis for the contention that clays inhibit hydrate formation. According to the PT equilibrium lines in Figure 2, the Otay clay promoted MH formation slightly more than the Cheto clay over the entire clay concentration range. The shifts of pressure (ΔP) and temperature (ΔT) for both clays are not considerable but are sufficient to promote the formation of methane hydrate. At a clay mass fraction above 25 %, the promotional trend disappeared, implying that there exists a certain value of upper limit in the clay concentration for optimal IMH formation. During the present PT experiments, special care was taken to eliminate any residual water that possibly formed pure methane hydrate in an unfavorable inhibition state. Thus we determined the genuine stability boundary of methane hydrate in the clay interlayer region. The clay pores were completely saturated with water, and hydrate in principle lowers the water activity due to a capillary effect originating from geometrical constraints.[18−20]

As shown in Table 2, Cheto and Otay clays also contain regular pores of surface and internal space that may cause the equilibrium line to shift toward lower temperature and higher pressure conditions.[18−20] However, Otay clay with 3.85 nm pore size more strongly promoted methane hydrate formation relative to Cheto clay with 6.21 nm pore size. This implies that the thermodynamic promotion phenomenon occurring in the clay−water−methane matrix is more complex than expected. From the reference, the mobile exchangeable cation in the interlayer of Cheto clay is Ca^{2+}, but the Otay clay does not have a dominant interlayer cation.[15] Diverse compositions of exchangeable cations in clay minerals result in diverse colloidal, plastic, and other properties of clays upon interaction with the sur-

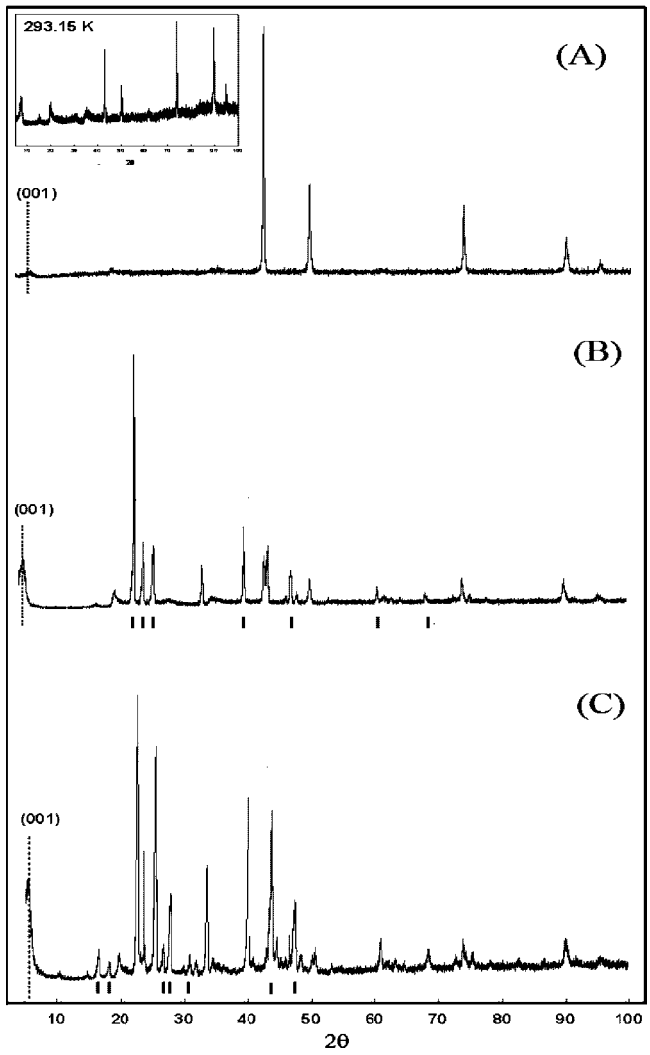

Figure 6. XRD patterns of (A) pure Cheto clay powder at (293.15 and 203.15) K, d-spacing(001) = 12.65 Å, (B) mass fraction of 25 % clay water suspension, d-spacing(001) = 15.38 Å (tick marks correspond to hexagonal ice (ih)), and (C) mass fraction of 25 % clay CH_4 hydrates, d-spacing(001) = 16.06 Å (tick marks correspond to structure I hydrate).

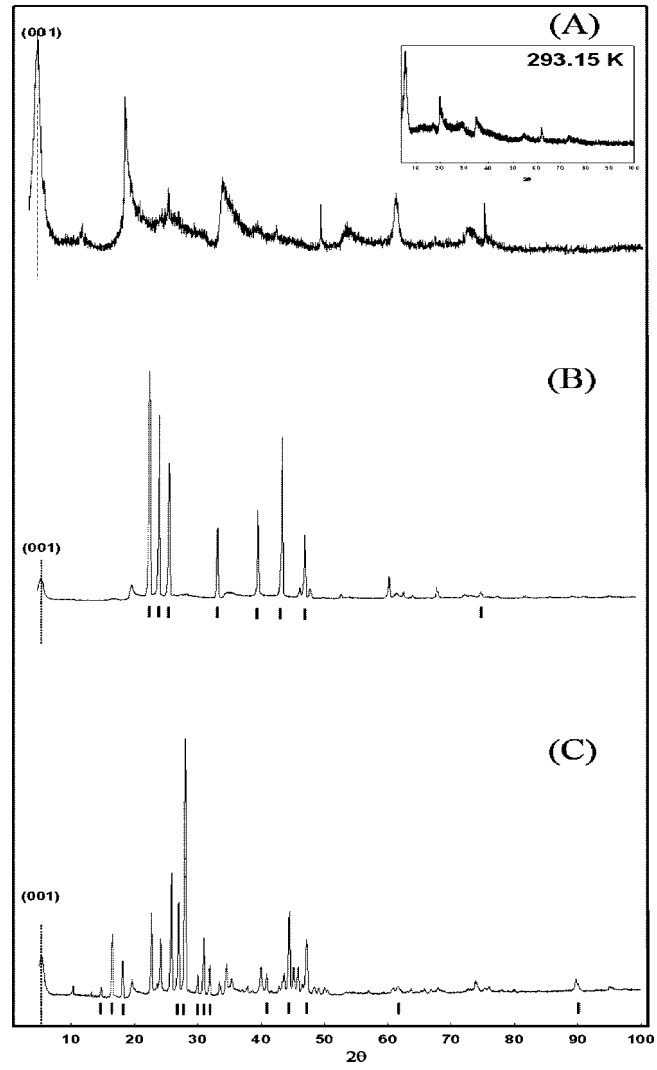

Figure 7. XRD patterns of (A) pure Otay clay powder at (293.15 and 203.15) K, d-spacing(001) = 13.97 Å, (B) mass fraction of 25 % clay water suspension, d-spacing(001) = 15.63 Å (tick marks correspond to hexagonal ice (ih)), and (C) mass fraction of 25 % clay CH_4 hydrates, d-spacing(001) = 16.11 Å (tick marks correspond to structure I hydrate).

rounding media.[16,17] From Figure 2, it is seen that the Cheto clay with interlayer Ca^{2+} exhibits a weaker promotion function for hydrate stability than the Otay clay. It indicates that the size and charge of the interlayer cation significantly might influence the entire IMH formation process, including crystal nucleation and growth. Therefore, we provisionally conclude from these preliminary results that the intercalation phenomena of IMH in the clay interlayer including mobile exchangeable cations might be too complex to reveal the key features of guest dynamics in the clay matrix and still on investigation now.

Structural and Spectroscopic Characteristics of IMH. First, we confirmed the reported result that the Raman bands at (2903 to 2915) cm^{-1} are assigned as the C−H vibration of sI methane[21] in small and large cages. The Raman spectra of the pure Cheto and Otay clay powders and intercalated methane hydrates were determined at 203 K in a range of (50 to 3600) cm^{-1} and are assigned according to the reported findings.[22,23] Most bands generated by lattice vibrations of both pure clays are centered at ≈100 cm^{-1}, 200 cm^{-1}, 275 cm^{-1}, ≈450 cm^{-1}, and 710 cm^{-1}, as shown in Figure 3(A), whereas the broad bands over (3100 to 3500) cm^{-1} in (B) originate from O−H vibration of the host water framework.[21] The bands between (200 and 710) cm^{-1} are considered to evolve from SiO_4 and Al_2O_3 lattices, respectively. We directed particular attention to the mobile cations in the interlayer below 100 cm^{-1}.[22,23] The XRD patterns of clay + MH clearly indicate that the IMH were a little swelled, causing the corresponding d-space increase, while clay peaks remain intact during intercalation. In contrast, the Cheto clay bands were almost identical for all clay samples. The ^{27}Al and ^{29}Si solid-state MAS NMR spectra indicate that there are no significant chemical shift differences between pure clays and intercalated clays, as shown in Figures 4 and 5. The Cheto montmorillonite structurally belongs to the 2:1 dioctahedral phyillosilicate, which is basically composed of a central octahedral sheet and two tetrahedral sheets. In the tetrahedral sheet, the individual silica tetrahedral is linked with three neighboring tetrahedrals to form hexagonal patterns in the layer plane. Using MAS NMR spectroscopy, it is possible to distinguish between octahedral and tetrahedral coordination of Al and to establish the different chemical environments of Si in aluminosilicate structures. The 2:1 phyillosilicates have Al ions centered near 0 ppm only in octahedral sites, as previously reported.[24,25] The ^{27}Al MAS NMR spectra of pure Cheto and Otay clay powders and intercalated methane hydrates show chemical shifts near 0 ppm, which are assigned as octahedral Al ions. Furthermore, the ^{29}Si MAS NMR spectra representing

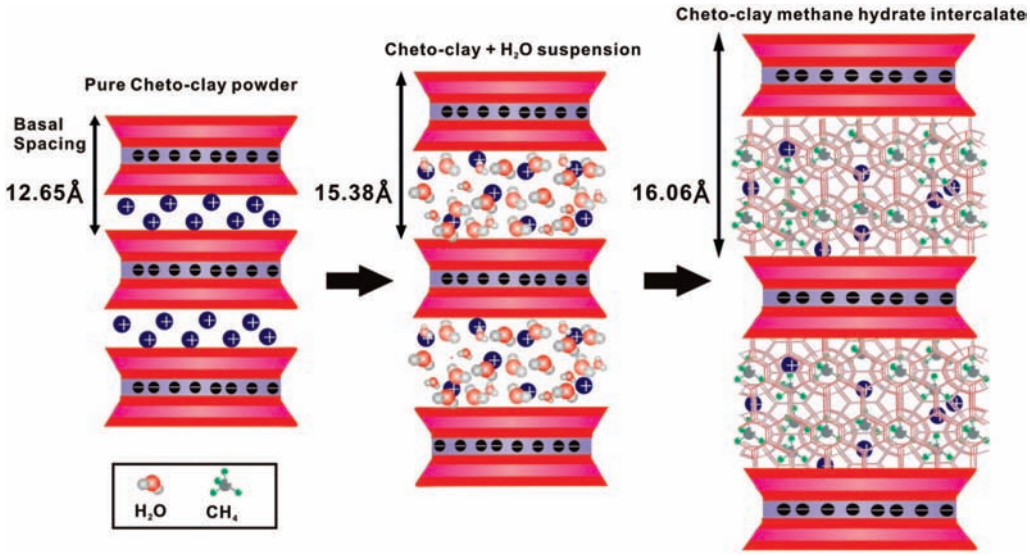

Figure 8. Shematic of the intercalated methane hydrate formation. During the IMH formation, interlayer distance was gradually extended.

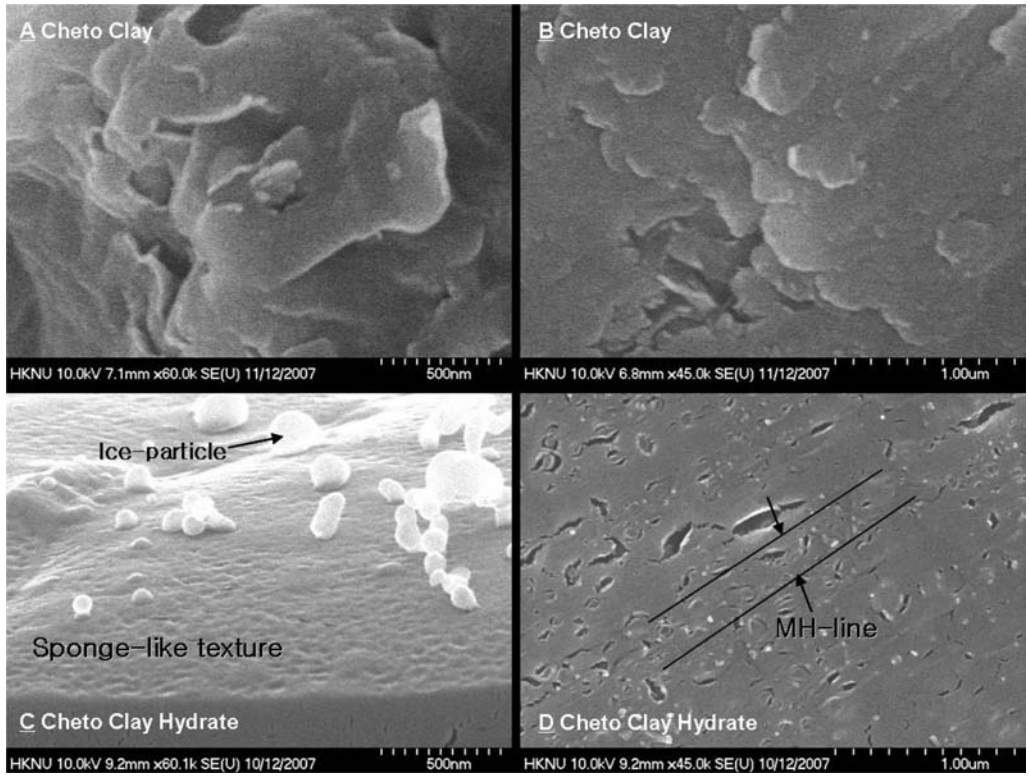

Figure 9. Cryo-SEM images of Cheto and the IMH Cheto clay surface morphology (A,C, simple surface; and B,D, flat frozen cut surface).

the tetrahedral environments show a chemical shift near −90 ppm for the Si atom surrounded by three other Si atoms in tetrahedral sheets. It is thus likely that Cheto and Otay clay layers preserve their structural stability during the formation of intercalated methane hydrate.

Low-temperature XRD patterns of both pure Cheto and Otay clay powders at 203.15 K are presented in Figures 6 and 7. The (001) diffraction pattern of the smectite clay group varies as a function of numerous factors, including the type of interlayer cations and relative humidity (RH).[26] For increased accuracy, all of the Cheto-type clays were kept in a desiccator to prevent water adsorption. The inset XRD patterns in the small box were determined for pure Cheto and Otay clay powders at 293.15 K. Both sI peaks for methane hydrate and ice peaks were assigned using CHECKCELL and GSAS. For the (001) basal plane peak, the interlayer d-spacing value of the pure Cheto clay was found to be 12.65 Å. This interlayer distance was gradually extended to 15.08 Å for the clay−water suspension and further increased to 16.06 Å for the intercalated methane hydrate. The schematic of the intercalated methane hydrate formation is shown in Figure 8. The Otay clay exhibited a similar swelling pattern, giving corresponding d-spacing values of (13.97, 15.63, and 16.11) Å. In the case of the Otay clay + methane hydrate system, the band intensity and shape around 100 cm^{-1} were significantly changed during methane hydrate formation, while the corresponding wavenumber was almost unchanged. This reflects the absence of structural transformation, which indirectly agrees with the results of the NMR ^{27}Al and ^{29}Si MAS NMR analyses. According to spectroscopic results obtained from Raman, NMR, and XRD analysis for Cheto and

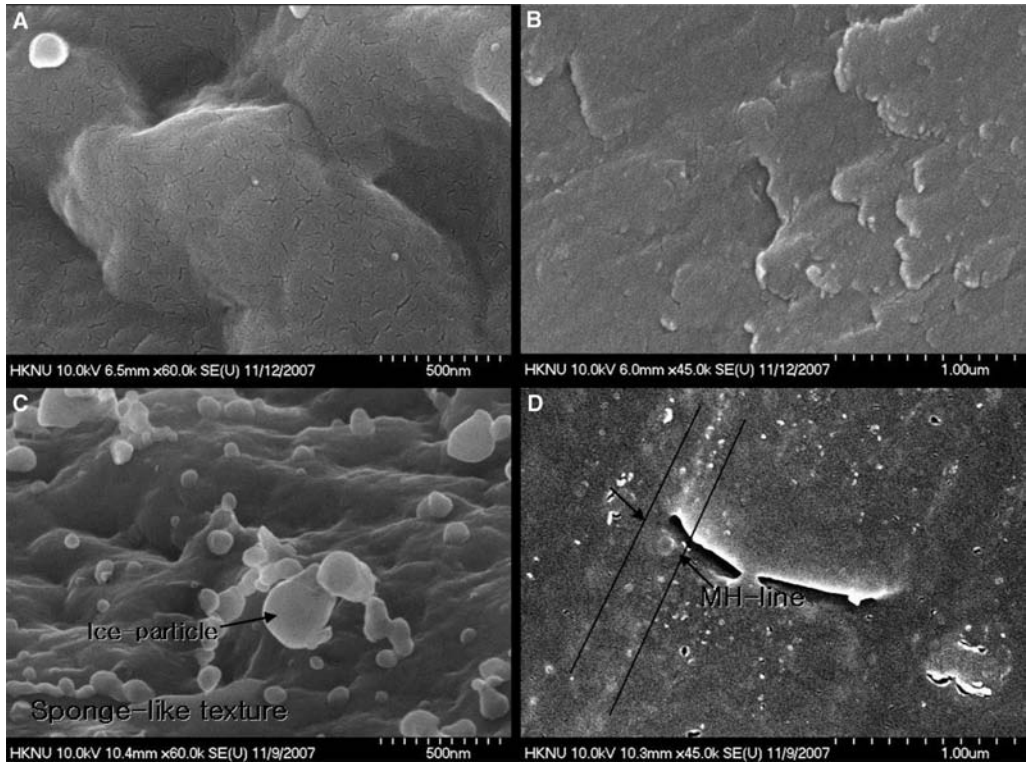

Figure 10. Cryo-SEM images of Otay and the IMH Otay clay surface morphology (A,C, simple surface; and B,D, flat frozen cut surface).

Otay clays, it could be concluded that the clay layer structure lattice (Al/Si) does not strongly interact with the intercalated methane hydrate. However, the interlayer cations are thought to play a role in promoting methane hydrate stability. These findings were also observed for the Otay clay samples.

To monitor topological changes of the clay surface after the formation of methane hydrate intercalated in the interlayer space of Cheto-type montmorillonites, we obtained Cryo-SEM images at low temperature, as shown in Figures 9 and 10. Scanning electron microscopy (SEM) offers a powerful technique for providing morphology information and elucidating the gas hydrate growth process. The surface morphologies of pure clays and IMH clays are shown in Figures 9 and 10: Figure 9(A) represents the pure Cheto clay (sample surface), Figure 9(B) the Cheto clay (flat frozen cut surface), Figure 9(C) the IMH Cheto clay (sample surface), Figure 9(D) the IMH Cheto clay (flat frozen cut surface), Figure 10(A) the pure Otay clay (sample surface), Figure 10(B) the Otay clay (flat frozen cut surface), Figure 10(C) the IMH Otay clay (sample surface), and Figure 10(D) the IMH Otay clay (flat frozen cut surface). Ice particles are found on the surface of the IMH Cheto and Otay clays, where the formed methane hydrates appear to be uniformly dense and are thought to have a sponge-like surface texture. The IMH Otay clay with larger surface area and smaller pore size appears to provide the well-developed methane hydrate morphology, compared to the IMH Cheto clay. Thin white lines across the plane are observed in Figure 9(D) and 10(D) and might be regarded as MH grain aggregates. In contrast, these white lines are not found for the pure Cheto and Otay clay powders in Figure 9(B) and 10(B). Stern et al. showed the natural surface morphology of methane hydrate growth,[27] but we attempted to observe the methane hydrate images taken at frozen cut surfaces. In the present approach, we have tried to provide the morphological patterns for the used clays simply only at the quite preliminary level, but the extensive research must be truly done to reveal the real nature of deep-sea floor methane hydrate sediments.

Table 3. Released Gas Volume per Water Content of Cheto and Otay Clay CH_4 Hydrate at a Mass Fraction of (25 and 80) % Concentration, Respectively

	Cheto type		Otay type	
mass fraction of clay (100 W)	25	80	25	80
methane contents/mL·g^{-1}	117.5	96.1	125.6	143.0

The amount of gas released from IMH clays is measured at different clay concentrations to understand the methane gas entrapped in IMH of both Cheto and Otay clays, and the results are presented in Table 3. It is noted that the amount of methane gas is around 120 mL of CH_4/g of hydrate for both Cheto and Otay clays at mass fractions of 25 %, but at a mass fraction of 80 %, it increased to 143.0 mL of CH_4/g of hydrate for Otay clay and decreased to 96.1 mL of CH_4/g of hydrate for Cheto clay. As we indicated in Figure 2 of phase equilibrium measurement, the Otay clay promoted the MH formation more than that of the Cheto clay, possibly due to the different interlayer cation effect. It might be suggested that these structural characteristics should affect the amount of methane gas entrapped in IMH. Further studies are under evaluation to elucidate the precise mechanism of methane hydrate formation in clay minerals and the effect of clay structure on phase behavior and structural characteristics.

Conclusions

In the present work, we measured the physicochemical properties of methane hydrates intercalated in clays. Diverse characteristics of both Wyoming- and Cheto-type montmorillonites were identified from the rheological behavior of the clays and chemical composition analysis. A promoting tendency was observed for IMH. However, for a clearer description, further detailed investigations need to be carried out to find the key influencing variables. The IMH morphology appears to be quite unique depending on the physicochemical properties of the clays. The direct release results suggest that IMH could be formed at

high concentrations of clay. This study aimed at performing experimental measurements of both clays and IMH properties, even though natural clay sediments might be quite different from simple clays.

Literature Cited

(1) Sloan, E. D., Jr. *Clathrate Hydrates of Natural Gases*, 2nd ed.; Marcel Dekker: New York, 1998.

(2) Lu, H.; Seo, Y. T.; Lee, J. W.; Moudrakovski, I.; Ripmeester, J. A.; Chapman, N. R.; Coffin, R. B.; Gardner, G.; Pohlman, J. Complex gas hydrate from cascadia margin. *Nature* **2007**, *445*, 303–306.

(3) Grim R. E. *Clay Mineralogy*, 2nd ed.; McGraw-Hill Book Company, 1968.

(4) Ouar, H.; Cha, S. B.; Wildeman, T. R.; Sloan, E. D., Jr. The formation of natural gas hydrates in water-based drilhng-fluids. *Chem. Eng. Res. Des.* **1992**, *70*, 48–54.

(5) Grim, R. E.; Kulbicki, G. Montmorillonite: high temperature reactions and classification. *Am. Mineral.* **1961**, *46*, 1329–1369.

(6) Cha, S. B.; Ouar, H.; Wildeman, T. R.; Sloan, E. D., Jr. A third-surface effect on hydrate formation. *J. Phys. Chem.* **1988**, *92*, 6492–6494.

(7) Sposito, G.; Skipper, N. T.; Sutton, R.; Park, S. H.; Soper, A. K.; Greathouse, J. A. Surface geochemistry of the clay minerals. *Proc. Natl. Acad. Sci. U.S.A.* **1999**, *96*, 3358–3364.

(8) Park, S. H.; Sposito, G. Do Montmorillonite Surfaces Promote Methane Hydrate Formation? Monte Carlo and Molecular Dynamics Simulations. *J. Phys. Chem. B* **2003**, *107*, 2281–2290.

(9) Cygan, R. T.; Guggenheim, S.; Koster van Groos, A. F. Molecular Models for the Intercalation of Methane Hydrate Complexes in Montmorillonite Clay. *J. Phys. Chem. B* **2004**, *108*, 15141–15149.

(10) Guggenheim, S.; Koster van Groos, A. F. New gas-hydrate phase: Synthesis and stability of clay-methane hydrate intercalate. *Geology* **2003**, *31*, 653–656.

(11) Kotkoskie, T. S.; Al-Ubaldi, B.; Wildeman, T. R.; Sloan, E. D., Jr. Inhibition of gas hydrates in water∼ based drilling muds. *SPE Drill. Eng.* **1992**, 130–136.

(12) Chuvilin, E. M.; Kozlova, E. V.; Makhonina, N. A.; Yakushew, V. S.; Dubinyak, D. V. Pecularities of methane hydrate formation/dissociation P/T conditions in sediments of different composition. *Proc. Fourth Int. Conf. Gas Hydrate* **2002**, 433–438.

(13) Lee, K. M.; Lee, H.; Lee, J. H.; Kang, J. M. CO_2 hydrate behavior in the deep ocean sediments; phase equilibrium, formation kinetics, and solubility. *Geophys. Res. Lett.* **2002**, *29*, 2034–2038.

(14) Englezos, P.; Hall, S. Phase equilibrium data on carbon dioxide hydrate in the presence of electrolytes, water soluble polymers and montmorillonite. *Can. J. Chem. Eng.* **1994**, *72*, 887–893.

(15) Selvam, A.; See, C. H.; Barkdoll, B.; Prasad, S.; O'Hver, J. *Proceeding of World Water & Environmental Resources Congress*, 2003.

(16) Volzone, C.; Garrido, L. B. The effect of some physico-chemical and mineralogical properties on the Na_2CO_3 activation of Argentine bentonites. *Appl. Clay Sci.* **1991**, *6*, 143–154.

(17) Volzone, C.; Garrido, L. B. Changes in suspension properties of structural modified montmorillonites. *Cerâmica* **2001**, *47*, 4–8.

(18) Handa, Y. P.; Stupin, D. Thermodynamic properties and dissociation characteristics of methane and propane hydrates in 70-. ANG.-radius silica gel pores. *J. Phys. Chem.* **1992**, *96*, 8599–8603.

(19) Uchida, T.; Ebinuma, T.; Ishizaki, T. Dissociation Condition Measurements of Methane Hydrate in Confined Small Pores of Porous Glass. *J. Phys. Chem. B* **1999**, *103*, 3659–3663.

(20) Uchida, T.; Takeya, S.; Kamata, Y.; Ikeda, I. Y.; Nagao, J.; Ebinuma, T.; Narita, H.; Zatsepina, O.; Buffett, B. A. Spectroscopic Observations and Thermodynamic Calculations on Clathrate Hydrates of Mixed Gas Containing Methane and Ethane: Determination of Structure, Composition and Cage Occupancy. *J. Phys. Chem. B* **2002**, *106*, 12426–12431.

(21) Subramanian, S.; Kini, R. A.; Dec, S. F.; Sloan, E. D., Jr. Evidence of structure II hydrate formation from methane+ethane mixtures. *Chem. Eng. Sci.* **2000**, *55*, 1981–1999.

(22) Frost, R. L.; Rintoul, L. Lattice vibrations of montmorillonite: an FT Raman and X-ray diffraction study. *Appl. Clay Sci.* **1996**, *11*, 171–183.

(23) Bishop, J. L.; Murad, E. Characterization of minerals and biogeochemical markers on Mars: A Raman and IR spectroscopic study of montmorillonite. *J. Raman Spectrosc.* **2004**, *35*, 480–486.

(24) Sanz, J.; Serratosa, J. M. High-resolution MAS-NMR spectra of phyllosilicates. *J. Am. Chem. Soc.* **1984**, *106*, 4790–4793.

(25) Sanz, J.; Robert, J. L. Influence of structural factors on ^{29}Si and ^{27}Al NMR chemical shifts of phyllosilicates 2:1. *Phys. Chem. Miner.* **1992**, *19*, 39–45.

(26) Chipera, S. J.; Bish, D. L. Baseline studies of the clay minerals source clays: powder X-ray diffraction analyses. *Clays Clay Miner.* **2001**, *49*, 398–409.

(27) Stern, L. A.; Kirby, S. H.; Circone, S.; Durham, W. B. Scanning Electron Microscopy Investigations of Laboratory-grown Gas Clathrate Hydrates Formed from Melting Ice, and Comparison to Natural Hydrates. *Am. Mineral.* **2004**, *89*, 1162–1175.

Received for review November 6, 2008. Accepted February 16, 2009. This work was supported by the Korea Science and Engineering Foundation (KOSEF) through the National Research Laboratory. Program funded by the Ministry of Education, Science and Technology (No.R0A-2005-000-10074-0(2008)), and "Identifying the Natural Phenomenon of Methane Hydrate Formation in Clay and Sand Layers for recovering of gas hydrate" funded by the Ministry of Knowledge, Economy of Korea, also partially funded by the Brain Korea 21 Project. This work was supported by the Korea Science and Engineering Foundation (KOSEF) grant (WCU program, 31-2008-000-10055-0) funded by the Ministry of Education and Science and Technology (MEST).

JE800833Y